IJNAOE
©SNAK, 2014

Int. J. Nav. Archit. Ocean Eng. (2014) 6:151~161
http://dx.doi.org/10.2478/IJNAOE-2013-0169
pISSN: 2092-6782, eISSN: 2092-6790

An experimental assessment of resistance reduction and wake modification of a KVLCC model by using outer-layer vertical blades

Nam Hyun An[1], Sang Hoon Ryu[2], Ho Hwan Chun[3] and Inwon Lee[3]

[1]*Department of Shipbuilding and Marine Engineering, Koje College, Gyeongnam, Korea*
[2]*Flutek Ltd., Gyeongnam, Korea*
[3]*Global Core Research Center for Ships & Offshore Plants (GCRC-SOP), Pusan National University, Busan, Korea*

ABSTRACT: *In this study, an experimental investigation has been made of the applicability of outer-layer vertical blades to real ship model. After first devised by Hutchins and Choi (2003), the outer-layer vertical blades demonstrated its effectiveness in reducing total drag of flat plate (Park et al., 2011) with maximum drag reduction of 9.6%. With a view to assessing the effect in the flow around a ship, the arrays of outer-layer vertical blades have been installed onto the side bottom and flat bottom of a 300k KVLCC model. A series of towing tank test has been carried out to investigate resistance (C_{TM}) reduction efficiency and improvement of stern wake distribution with varying geometric parameters of the blades array. The installation of vertical blades led to the C_{TM} reduction of 2.15~2.76% near the service speed. The nominal wake fraction was affected marginally by the blades array and the axial velocity distribution tended to be more uniform by the blades array.*

KEY WORDS: Energy efficient ship; Skin frictional drag reduction; Outer-layer vertical blades; Effective power; Turbulent boundary layer; Wake.

INTRODUCTION

Recent increase of oil price has triggered a significant change in the ship design trends, the energy saving design. The efforts to achieve energy efficient ship are divided into two categories; drag reduction and propulsion efficiency enhancement. Historically, more attention has been paid to the hull form optimization toward the reduction of wavemaking resistance than the turbulence control for the frictional drag reduction. However, the frictional drag accounts for about 70~80% of total drag of slow and full hull ships. This makes the frictional drag reduction significant for the energy saving design.

The frictional drag of ship is attributed to the wall shear stress of the turbulent boundary layer flow around the hull surface. The wall shear stress of turbulent boundary layer is in turn closely associated with the organized coherent structures such as hairpin vortices in the turbulent boundary layer flow. Various strategies of turbulent flow control toward either destruction or attenuation of such organized coherent structures have been proposed during several decades. From the viewpoint of reliability, the passive techniques such as riblet (Walsh, 1980; Beckert and Bartenwerfer, 1989), compliant coating (Choi et al., 1997) and Large Eddy BreakUp device (LEBU) is more suitable for the marine application. Hefner et al. (1979) conducted the experiments with LEBU to reduce the skin friction downstream of the LEBU devices and achieved 24% of drag reduction compared

Corresponding author: *Inwon Lee*, e-mail: *inwon@pusan.ac.kr*

to undisturbed flat plate levels. The LEBU devices directly interact with and change the large eddy structures, thus interruptting the production loop and reducing the bursting events causing surface stress. Schoppa and Hussain (1998) claimed that the imposition of a large-scale vortical control flow into turbulent boundary layer flow could lead to promising skin-friction reductions.

Hutchins and Choi (2002) and Hutchins (2003) introduced the idea of the outer-layer vertical blades, an array of thin vertical plates in the turbulent boundary layer. This array chops off large scale coherent structures of turbulence, thereby disconnecting the link between outer and inner layers. The height and the spanwise spacing were varied to find optimal values. As seen in Fig. 1, the skin friction reduction effect attains a maximum of 30% when the height of the blade h is approximately 50% of the local boundary layer thickness δ at the position of the blade in the undisturbed boundary layer without blades ($h/\delta = 0.5$). In this case, this maximum occurs at the position of six boundary layer thickness downstream of the blade ($x/\delta = 6$). Recently Park et al. (2011) investigated the frictional drag reduction capability of the outer-layer vertical blades. Whilst Hutchins (2003) demonstrated only the reduction local skin friction effect in the downstream of the blades, the towing tank measurements of Park et al. (2011) clarified the practical applicability by considering the device drag of the blades. It was found that the outer-layer vertical blades array achieved maximum 9.6% drag reduction, as presented in Fig. 2.

The present study is an extension of the previous research of Park et al. (2011) with a view to assessing the feasibility of the outer-layer vertical blades for three-dimensional flow around a ship model. The blades arrays were attached on the flat surfaces of a KVLCC model and a series of model tests in towing tank were carried out to investigate the resistance (C_{TM}) reduction efficiency and the improvement of stern wake distribution with varying geometric parameters.

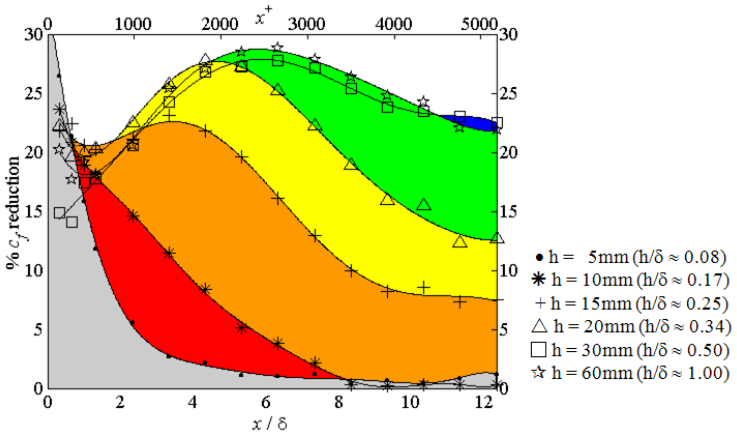

Fig. 1 Previous result of outer-layer vertical blades, effect of blade height on the local skin friction coefficient c_f reduction (Hutchins, 2003).

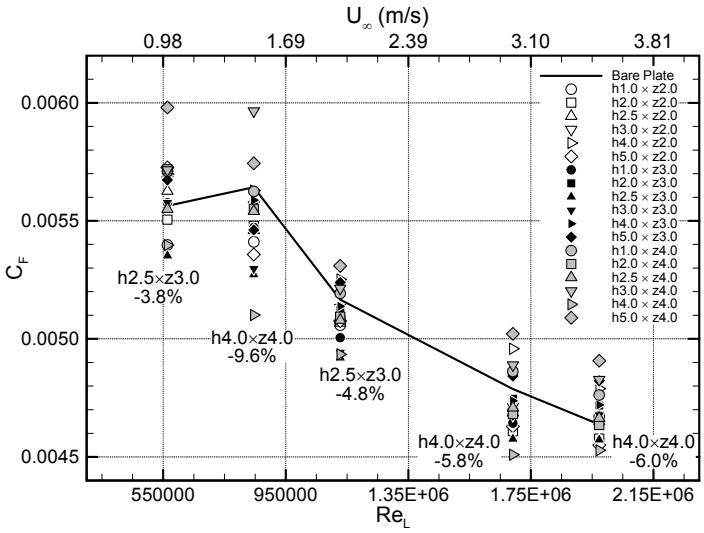

Fig. 2 Previous result of outer-layer vertical blades, skin-frictional drag coefficient versus Reynolds number for flat plate with blades array (Park et al., 2011).

EXPERIMENTAL METHODS

Model ship and flow conditions

For the present model test, 300*k* KVLCC was selected because plenty of data are available in the open literatures for this type. A KVLCC model with the scale ratio λ = 100 was manufactured out of wood with the principal particulars being listed in Table 1. As shown in Fig. 3, three rectangular slots were cut out at port, starboard and bottom sides of the hull and then covered with 10*mm* thickness acrylic panels. On each panel, 3*mm* wide groove was machined to facilitate the installation of blades array. The longitudinal location of the blades array (X_b) was selected approximately at the midsection, *i.e.*, the 10th station. This was made in order for the blades to be aligned to the incoming turbulent boundary layer on the midship parallel part of the hull. The spans of the arrays were set as long as possible within the widths of the acrylic panels. The port and starboard arrays were kept underwater with sufficiently small angle of attack to the incoming boundary layer flows in all test conditions.

Table 1 Principal particulars of 300*k* KVLCC.

Designation		Symbol (unit)	Ship	Model
Scale ratio		λ	1	100
Design speed		V	15.5(*kts*)	0.797(*m/s*)
Length between perpendiculars		LBP(*m*)	320.0	3.200
Length of waterline		LWL(*m*)	325.0	3.250
Breadth		B(*m*)	58.0	0.580
Draft	Forward	TF(*m*)	20.8	0.208
	Aft	TA(*m*)	20.8	0.208
Wetted surface area		WSA(m^2)	27,320.0	2.732
Displacement		DISV(m^3)	312,737.5	0.3127
Block coefficient		C_B	0.8101	

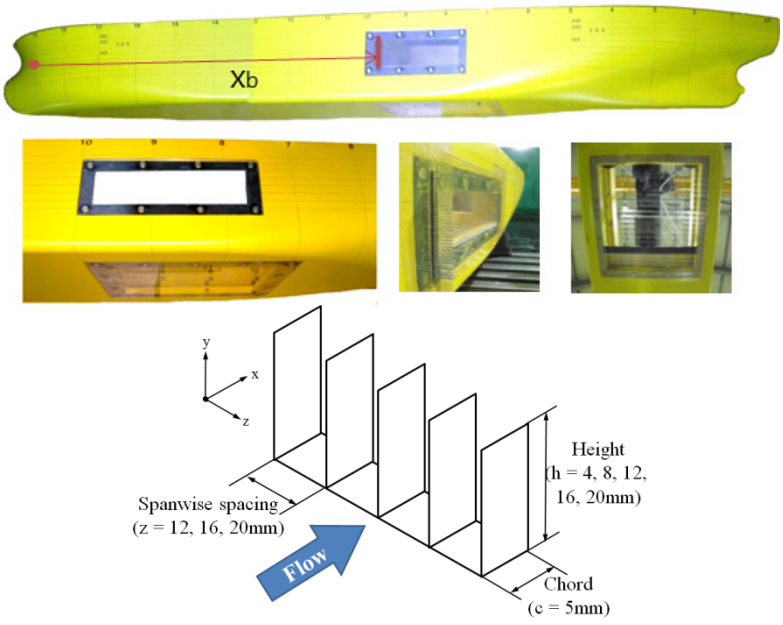

Fig. 3 Blades array installation system in the KVLCC model and geometry parameters of outer-layer blades array.

The vertical blades were constructed from 0.2*mm* thin stainless steel plate. The thickness of blades elements amounts to about 5 wall units ($t^+ = 5$) or 0.01δ. All vertical blades fit into the grooves of the socket, which were cut elaborately by water jet with 4*mm* interval. Fig. 3 illustrates the geometric parameters of the outer-layer vertical blades, height h, spanwise spacing z and chord length c. In the previous research of Park et al. (2011), the optimal height h was found to scale with the outer variables such as the boundary layer thickness δ. In this study, the blade height h was varied as 4, 8, 12, 16 and 20*mm* while the spanwise spacing z had the values of 12, 16 and 20*mm*. In designing those geometric parameters, it was required to estimate the boundary layer parameters at the location of the blades array. This was done by employing the empirical correlation of Schlichting and Gersten (2000) as follows;

$$\frac{\delta U_\infty}{\nu} = 0.14\frac{\left(Re_x - Re_{x0}\right)}{\ln\left(Re_x - Re_{x0}\right)}G\left(\ln Re_x\right),\quad G\left(\ln Re_x\right) = 1.5 \tag{1}$$

Here, Re_{x0} corresponds to the Reynolds number of the fictitious origin and the value $Re_{x0} = 1.5\times10^5$ was used. The value of the streamwise distance x is given as X_b = 1.6*m*, which is the distance between turbulence promoting studs near FP and the leading edge of blades. In addition, the local skin friction coefficient and consequent calculation of the friction velocity u_τ for the inner scaling was based on the correlation $c_f(x) = 0.455/\{\ln(0.06\,Re_x)\}^2$ given by White (1991). Table 2 presents flow conditions calculated at speeds near the design speed of 15.5*knots*.

Table 3 (a) and (b) represent the nondimensional blade height with respect to the varying freestream velocity based on the outer scaling h/δ and the inner scaling $u_\tau h/\nu$, respectively. Similar data are tabulated in Table 4 (a) and (b) regarding the nondimensional blade spacing, z/δ and $u_\tau z/\nu$. The blade height was chosen to be smaller than the boundary layer thickness δ. According to Park et al. (2011), blades protruding out of the boundary layer contribute to the device drag only without any skin friction reduction effect. In this study, a total of 15 combinations resulting from 5 heights and 3 spacings were selected for towing tank. Each array is referred to by the blade height and the spanwise spacing, *i.e.*, h16z12 corresponds to the array with the blade height and the spacing being 16*mm* and 12*mm*, respectively. In Fig. 4, five blades arrays (h4z16, h8z16, h12z16, h16z16 and h20z16) are shown.

Table 2 Flow condition in the present study.

Model speed V_m (*m/s*) Ship speed V_S (*knots*)	0.746 14.5	0.772 15.0	**0.797** **15.5**	0.823 16.0	0.849 16.5
Re_x	9.137×10^5	9.455×10^5	**9.761×10^5**	1.008×10^6	1.040×10^6
δ(*mm*)	20.73	20.81	**20.87**	20.93	20.99
$\delta^+ = \delta u_\tau/\nu$	530.5	549.6	**567.8**	586.7	605.5
$c_f(x)$	3.821×10^{-3}	3.797×10^{-3}	**3.775×10^{-3}**	3.753×10^{-3}	3.732×10^{-3}
u_τ (*m/s*)	0.0334	0.0345	**0.0355**	0.0366	0.0377

Table 3 Nondimensional blade height with respect to varying freestream velocity using.

(a) Outer scaling, h/δ.

V_m (*m/s*) h(*mm*)	0.746 (14.5*kts*)	0.772 (15.0*kts*)	**0.797** **(15.5*kts*)**	0.823 (16.0*kts*)	0.849 (16.5*kts*)
4	0.193	0.192	**0.192**	0.191	0.191
8	0.386	0.384	**0.383**	0.382	0.381
12	0.579	0.577	**0.575**	0.573	0.572
16	0.772	0.769	**0.767**	0.764	0.762
20	0.965	0.961	**0.958**	0.955	0.953

(b) Inner scaling, $h^+ = u_\tau h/\nu$.

h(*mm*) \ V_m (*m/s*)	0.746 (14.5*kts*)	0.772 (15.0*kts*)	**0.797 (15.5*kts*)**	0.823 (16.0*kts*)	0.849 (16.5*kts*)
4	102	106	**109**	112	115
8	205	211	**218**	224	231
12	307	317	**326**	336	346
16	409	423	**435**	448	462
20	512	528	**544**	561	577

Table 4 Nondimensional blade spacing with respect to varying freestream velocity using.

(a) Outer scaling, z/δ.

z(*mm*) \ V_m (*m/s*)	0.746 (14.5*kts*)	0.772 (15.0*kts*)	**0.797 (15.5*kts*)**	0.823 (16.0*kts*)	0.849 (16.5*kts*)
12	0.579	0.577	**0.575**	0.573	0.572
16	0.772	0.769	**0.767**	0.764	0.762
20	0.965	0.961	**0.958**	0.955	0.953

(b) Inner scaling, $z^+ = u_\tau z/\nu$.

z(*mm*) \ V_m (*m/s*)	0.746 (14.5*kts*)	0.772 (15.0*kts*)	**0.797 (15.5*kts*)**	0.823 (16.0*kts*)	0.849 (16.5*kts*)
12	307	317	**326**	336	346
16	409	423	**435**	448	462
20	512	528	**544**	561	577

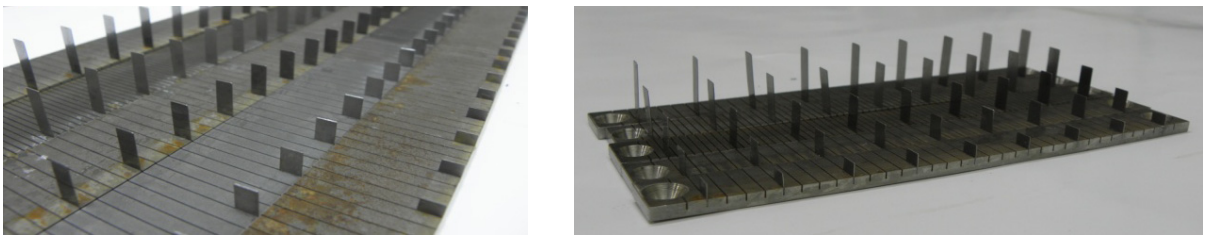

Fig. 4 Photographs of outer-layer blades arrays used in the present study.

Towing tank experiment

The measurements were performed in the towing tank facility of Pusan National University. The dimension of the towing tank is 100*m* in length, 8*m* in width and 3.5*m* in depth. The resistance of KVLCC model was measured at nine towing speeds from 11*knots* to 16.5*knots*. While the speed interval was set at 1.0*knot* from 11 to 14*knots*, it was set as 0.5*knot* from 14.5 to 16.5*knots*. Throughout the experiment, care was exercised to minimize the measurement uncertainty by carrying out drag measurements four times for each test condition. In addition to the resistance measurement, nominal stern wake distribution was investigated at the propeller plane by a 5-hole pitot-tubes rake. The diameter of the propeller plane was 0.1*m* (1/100 scale). Three dimensional wake velocity components were measured at the positions of 0.3*R*, 0.5*R*, 0.7*R*, 0.9*R* and 1.1*R* in the propeller plane. Fig. 5 indicates the 5-hole pitot tubes rake and differential pressure gauges used in this study.

Fig. 5 Photographs of wake measurement setup.

RESULTS AND DISCUSSIONS

Effect of geometric variation of vertical blades on the resistance reduction in model scale

In Fig. 6, the resistance R_{TM} of the baseline case, bare hull without the vertical array in the present study is plotted as a function of model speed V_M(*m/s*). Uncertainty estimates for the total drag measurements was made by the standard procedure of Moffat (1982). The 95% precision confidence limits for mean statistic were calculated by Student's t value for four repeatability tests (2 degrees of freedom). Total uncertainty of this system mainly consisted of the uncertainties from the force gages (max ± 0.25%), the water temperature and the towing carriage speed (max ±1%). The measurement uncertainty in the R_{TM} ranged ±1.23 to ±0.76%, as depicted in Fig. 6.

Fig. 7 shows the total drag coefficient C_{TM} $\left(= R_{TM}/0.5\rho V_M^2 S_M\right)$ of total 15 cases with varying blades configuration along with the bare hull case. It is seen that the installation of the vertical array led predominantly to the reduction of C_{TM} with some exceptions at lower speeds. Since the vertical blades array is located below the waterline, the variation of resistance is caused by the change of turbulent boundary layer around the ship hull. Therefore, the C_{TM} reduction in the present study results from the skin frictional drag reduction by vertical blades array identified by Park et al. (2011). The positive and negative figure at each ship speed represent maximum percentage of C_{TM} increase and decrease, respectively. A closer inspection of Fig. 7 indicates that maximum reduction of C_{TM} becomes reasonably uniform for speeds V_M over 0.66*m/s* (corresponding to V_S > 13*knots*). Near the design speed, between 0.7 7*m/s* and 0.82*m/s* (corresponding to V_S = 15~16*knots* in full scale), the blades array led to maximum C_{TM} reduction of 2.15~2.76%. It is found that difference in blades geometry causes variation of resistance performance. For instance, the array h16z20 (16*mm* in height and 20*mm* in spanwise spacing) led to resistance reduction of 2.28%, whilst the array h12z12 gave resistance increase of 0.16% at design speed.

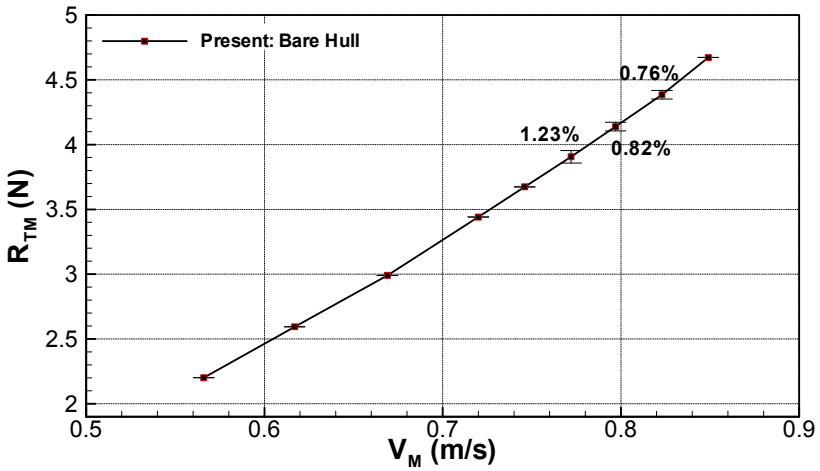

Fig. 6 Total resistance of bare hull without vertical array.

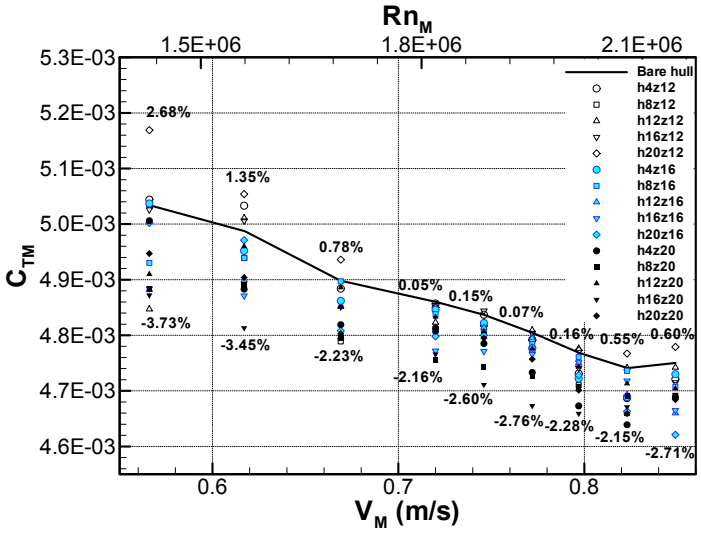

Fig. 7 C_{TM} versus Reynolds number with various blade arrays.

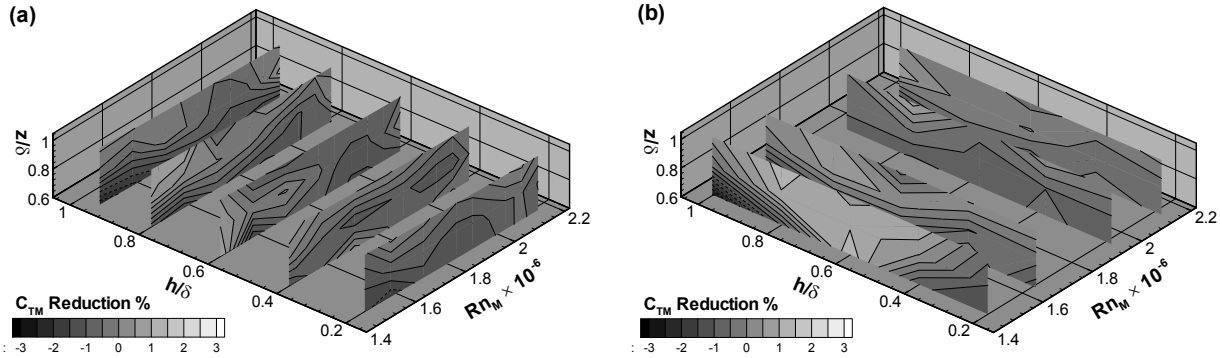

Fig. 8 Contour plots of percentage C_{TM} reduction in nondimensional geometry parameter space; (a) Plots with constant blade height, (b) Plots with constant model speed V_M.

In order to delineate the effect of blades geometry on C_{TM}, the percentage C_{TM} reduction $(1 - C_{TM} / C_{TM0})\times 100$ is depicted in Fig. 8 in a parameter space of h/δ, z/δ and Reynolds number of model Rn_M. The C_{TM} of bare hull is noted as C_{TM0}. The positive values correspond to C_{TM} reduction. The geometric parameters are nondimensionalized using outer scaling method. This is because the optimal height h was found to scale with the outer variables such as the boundary layer thickness δ (Park et al., 2011). As seen, three-dimensional parameter spaces are divided to subplanes where the 2-D contour plots are drawn with one parameter being fixed. At a first glance, the C_{TM} reduction effect is most noticeable for the lowest speed near 0.57*m/s* (corresponding to V_S = 11*knots*). At higher speeds, local maxima of the contours are found, implying that there is a certain relationship for an optimal geometry of blades array. A closer inspection of Fig. 8 reveals that h/δ and z/δ at local maxima of C_{TM} reduction is linearly correlated with each other. For instance, h/δ = z/δ = 0.6 and 0.8 show local maxima of C_{TM} reduction for V_M = 0.64 and 0.72*m/s* (V_S = 12.5 and 14*knots*). The dependence of C_{TM} reduction on nondimensional blade height h/δ is given in Fig. 9 at fixed z/δ. It is notable that the same h and z values give different nondimensional parameters h/δ and z/δ according to the variation of model speed. In Fig. 9, the considerable scatter between curves makes it difficult to extract a decisive tendency of C_{TM} reduction on h/δ. However, it is observed that the C_{TM} reduction tend to decline after a certain value of h/δ. For z = 12*mm* (z/δ ~ 0.6) in Fig. 9(a), the peak of C_{TM} reduction is found near h/δ = 0.4~0.6, while the corresponding optimal h/δ is located near h/δ = 0.8 for z = 16*mm* (z/δ ~ 0.8) in Fig. 9 (b). On the other hand, for z = 20*mm* (z/δ ~ 1.0) in Fig. 9 (c), the C_{TM} reduction drops after h/δ = 0.8. This supports the linear correlation between optimal h/δ and z/δ up to a certain threshold value, which is also consistent with the flat plate skin frictional drag measurement result (Park et al., 2011). As previously addressed by Park et al. (2011), this proportional relationship is based on the balance between mutually competing mechanisms of the attenuaiton of turbulence and the augmentation of device drag.

As mentioned in the introduction, the local skin friction reduction by means of vertical blades array was first demonstrated by Hutchins and Choi (2002) and Hutchins (2003). According to Fig. 1 showing their results, the local skin friction reduction effect persists up to $x^+ \approx 5{,}000$ ($x/\delta \approx 12$). It is also seen that the maximum local skin friction reduction becomes saturated for blade height $h/\delta > 0.5$. However, from the aspect of downstream persistence, it is implied that the higher blade height, the longer is the skin friction reduction sustained. There are two factors affecting the resistance reduction by the vertical blades in the present study. First, the total drag reduction is an integrated effect of local skin friction reduction along the downstream distance. Second, it is notable that the distance between the vertical blades array to stern corresponds to approximately 80δ in the present study. These factors account for the optimal height $h/\delta = 0.6 \sim 0.8$ observed in this study.

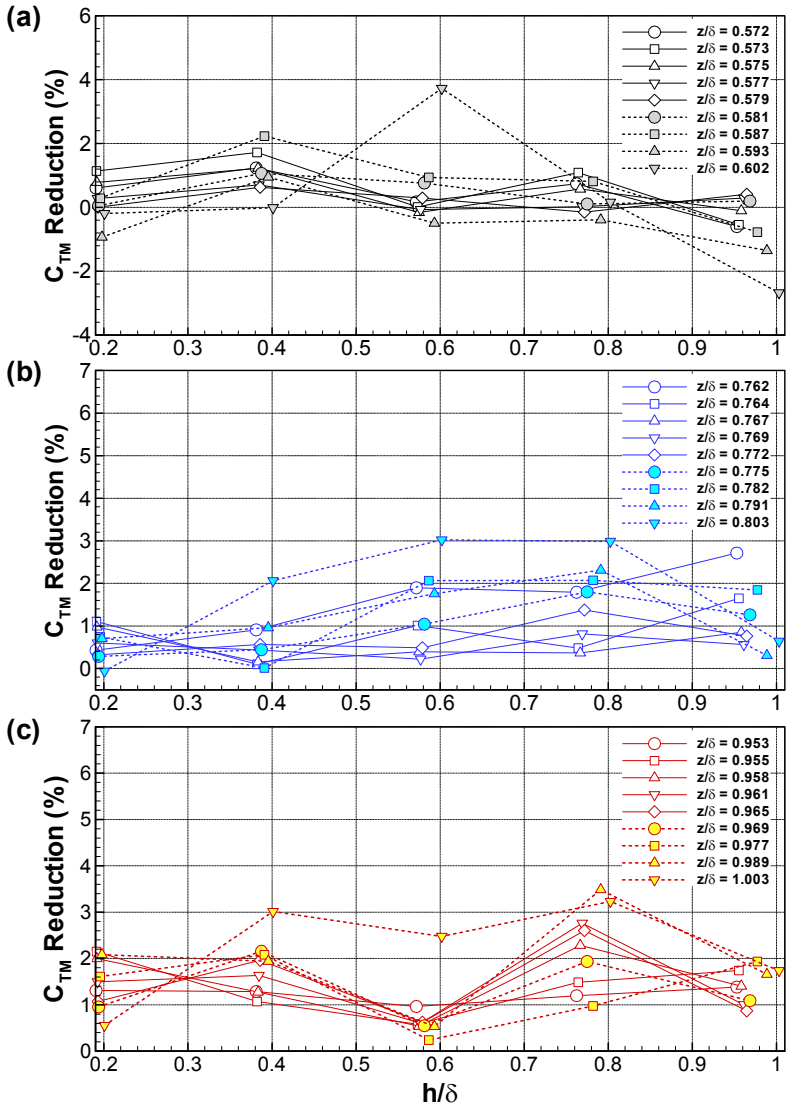

Fig. 9 Effect of blade height on percentage C_{TM} reduction (a) z = 12*mm*, (b) z = 16*mm*, (c) z = 20*mm*.

Effect of geometric variation of vertical blades on the wake distribution

In the present study, assessment has been extended to the wake distribution affected by the vertical blades array. This is based on the assumption that the change in the turbulent boundary layer which led to the drag reduction might as well affect the wake distribution. Fig. 10 illustrates such variations in wake distributions for a couple of blade configurations, h4z20 and h20z20, in comparison with the wake in bare hull case. The nominal wake fractions w_n in both cases are shown to decrease, but only slightly. The wake distributions also remain essentially the same with slightly noticeable acceleration of axial velocity component V_x (plotted in colored contours) in the dead water region near $\theta = 0°$. Taking the distance between the blades array

and the propeller plane, the marginal effect of blades on nominal wake is quite natural. With a view to investigating the effect of blades array on the wake flow, the axial velocity distributions along the azimuth angle at r = 0.7*R* for all blade cases are plotted against that for the bare hull case in Fig. 11. For all cases, it is discernible that the axial flow is accelerated in the range of 0° ≤ θ ≤ 30°, whereas the deceleration takes place for 60° ≤ θ ≤ 160°. In other words, the wake flow becomes more uniform with the presence of blades array.

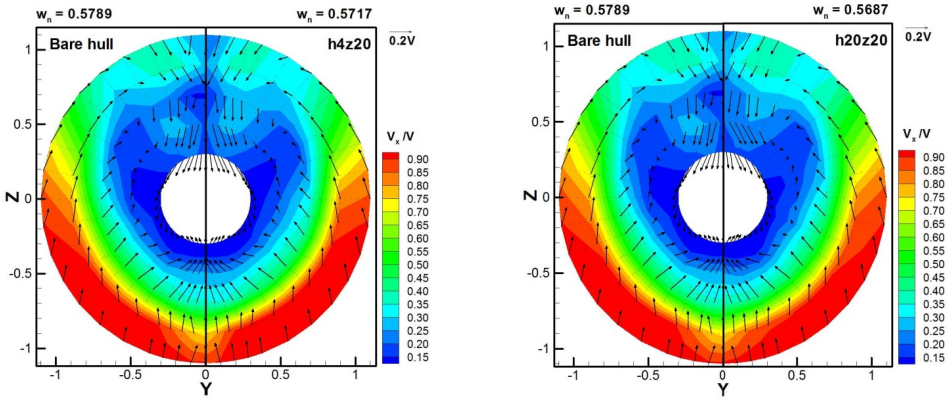

Fig. 10 Comparison of wake distribution for representative blade configurations.

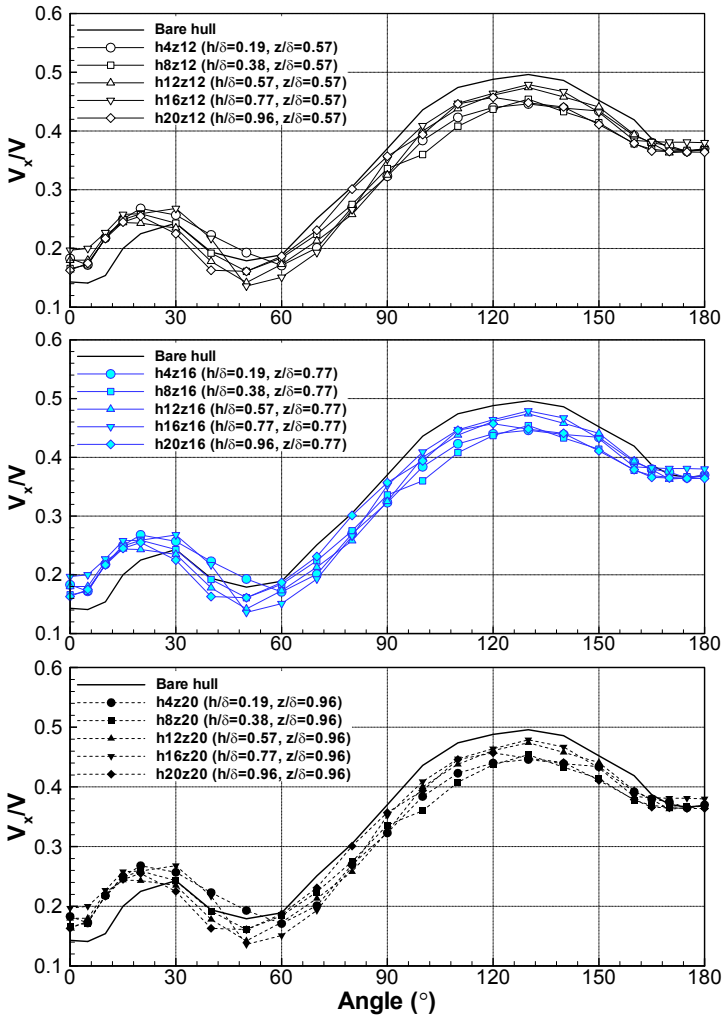

Fig. 11 Axial velocity distributions at 0.7*R* for each spanwise blade spacing (a) z = 12*mm*, (b) z = 16*mm*, (c) z = 20*mm*.

Fig. 12 gives percentage wake fraction reduction $(1 - w_n/w_{no})\times 100$ as a function of nondimensional blade height h/δ for fixed nondimensional blade spacing z/δ. Here, w_{no} refers to the wake fraction for bare hull case with $w_{no} = 0.5789$. No conspicuous trend is found, which implies that the influence of vertical blades is not dominant enough to make a significant change in wake flow. In the overall, the effect of vertical blades on wake distribution is only marginal. Installing the blades array nearer to the propeller would lead to substantial change in wake, but that would in turn diminish the resistance reduction effect because the area of downstream influenced area becomes smaller.

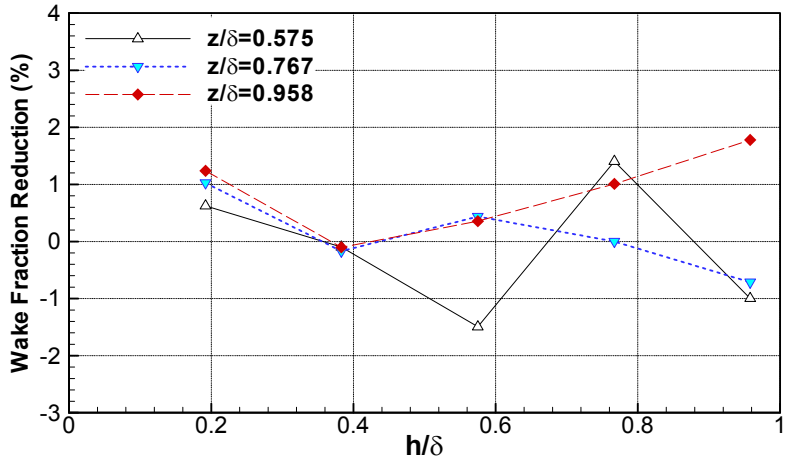

Fig. 12 Percentage wake fraction reduction against nondimensional blade height.

CONCLUSIONS

In the present study, an experimental assessment in towing tank has been made of the resistance reduction and wake modification capability of the outer-layer vertical blades, which is attached to the mid-section of a 300*k* KVLCC model ship. The present study is a sequel to the flat plate skin frictional drag reduction research using the vertical blades array by Park et al. (2011). The blade geometry was designed to follow the outer scaling based on the boundary layer thickness δ, which was found to be effective by Park et al. (2011). The installation of vertical blades led to the resistance (C_{TM}) reduction of 2.15~2.76% near the service speed, while the resistance reduction was found to be 2.15~3.73% in the entire range of ship speed under consideration. The linear correlation between optimal blade height h/δ and spanwise spacing z/δ is corroborated again in the model ship experiment. The resistance reduction effect becomes saturated as the nondimensional blade height h/δ approaches 1, which is consistent with the tendency in the previous research (Park et al., 2011). The nominal wake fraction was affected marginally by the blades array and the axial velocity distribution became more uniform by the blades array. The minor change of the wake due to the blades array is accounted for the limited downstream influence. In the overall, the drag reduction capability of the outer-layer vertical blades has been manifested by the present model ship experiment. It is remarkable that the present outer-layer vertical blades, unlike most existing hull appendages, could contribute to the improvement of energy efficiency through the resistance reduction.

It is worthwhile to mention that the present vertical blades array has a scaling issue arising from the Reynolds number dependence. Together with the previous study of Park et al. (2011), however, it has been consistently found that the influence of the present outer-layer vertical blades on the boundary layer flow scales with the outer variable, *i.e.*, the boundary layer thickness δ. This strongly implies that the present vertical blades may well be applied to full scale ship to obtain the similar effects as those found in the model study, provided the geometry is designed after the local boundary layer thickness. As addressed in the previous study, the outer scaling device as the present vertical blades array is advantageous in the application point of view. Whilst the inner scale device such as riblets requires sub-millimeter scale which is prohibitively small for real ship application, the present blades array remain in the feasible manufacturing scale of the boundary layer thickness. For instance, the boundary layer thickness at the midship of KVLCC for the design speed of 15.5*knot* is estimated to be 1.3*m*. Therefore, typical optimal blade height of 0.6 boundary layer thickness amounts to 0.79*m*. Considering the streamwise distribution of the local skin friction reduction shown in Fig. 1, the skin frictional reduction effect of the vertical blades array persists up to 20 boundary layer

thicknesses downstream. Combining $\delta = 1.3m$ in full scale ship with this leads to the estimates for the effective downstream zone of approximately 10% of ship length in full scale. After this downstream length, the installation of an additional blades array, which needs to be appropriately scaled with the local boundary layer thickness, could lead to an additional skin frictional drag reduction. Although the effect of single blades array in the present study seems to be marginal, it is thus envisaged that the installation of blades arrays at multiple streamwise locations would give rise to more noticeable resistance reduction capability.

ACKNOWLEDGEMENTS

This work was supported by the National Research Foundation of Korea (NRF) grant funded by the Korea government (MSIP) through GCRC-SOP (No. 2011-0030013).

REFERENCES

Beckert, D.W. and Bartenwerfer, M., 1989. The viscous flow on surfaces with longitudinal ribs. *Journal Fluid Mechanics*, 206, pp.105-129.

Choi, K.S., Yang, X., Clayton, B.R., Glover, E.J., Atlar, M., Semenov, B.N. and Kulik, V.M., 1997. *Turbulent drag reduction using compliant surfaces*. Proceedings of the Royal Society of London, 453(1965), pp.2229-2240.

Hefner, J.N., Weinstein, L.M. and Bushnell, D.M., 1979. Large-Eddy breakup scheme for turbulent viscous drag reduction. Paper of the Symposium on Viscous Drag Reduction. *In: Viscous flow drag reduction; Symposium*, Dallas, Texas, 7~8 November 1979, p.110-127.

Hutchins, N., 2003. *An investigation of larger-scale coherent structures in fully developed turbulent boundary layers*. Ph.D. University of Nottingham.

Hutchins, N. and Choi, K.S., 2002. Towards a greater understanding of turbulent skin friction reduction. *Proceedings of ASME FEDSM'02 2002 ASME Fluids Engineering Division Summer Meeting*, Montreal, Quebec, Canada, 14-18 July 2002, Paper No. FEDSM2002-31060, pp.1449-1454.

Moffat, R.J., 1982. Contributions to the theory of single-sample uncertainty analysis. *Trans ASME Journal Fluids Engineering*, 104, pp.250-260.

Park, H., An, N.H., Hutchins, N., Choi, K.S., Chun, H.H. and Lee, I., 2011. Experimental investigation on the drag reducing efficiency of the outer-layer vertical blades. *Journal Marine Science Technology*, 16(4), pp.390-401.

Schlichting, H. and Gersten, K., 2000a. *Boundary layer theory*. 8th Ed. Berlin: Springer-Verlag.

Schoppa, W. and Hussain, F., 1998. Genesis of longitudinal vortices in near-wall turbulence. Meccanica, 33, pp.489-501.

Walsh, M., 1980. Drag characteristics of V-groove and transverse curvature riblets. *Symposium on Viscous flow drag reduction,* Dallas, TX, 7-8 November 1979, pp.168-184.

White, F.M., 1991. *Viscous fluid flow*. 2nd Ed. New York: McGraw Hill.